# 21 cm OBSERVATIONS OF NGC 45

By B. M. Lewis*

[Manuscript received 2 August 1971]

*Abstract*

Observations of NGC 45 have been made at a wavelength of 21 cm using the radio telescope at Parkes. Line profiles have been measured for a grid of 44 points spaced at intervals of 6′ arc. From the measurements the mass of neutral hydrogen is calculated to be $8{\cdot}2\times10^8 M_\odot$, assuming a distance of 3 Mpc. A simple self-consistent model is determined by computing line profiles to compare directly with the observations. This enables the rotation curve to be corrected for the first-order effects of beam smoothing and results in a total limiting mass of $2{\cdot}5\times10^{10} M_\odot$.

## I. Introduction

The object NGC 45 has been used by Sandage (1961) as an example of a well-formed Sc galaxy of low surface brightness. More distant galaxies can be seen through the interarm regions since NGC 45 appears to be almost free of dust. From a consideration of its position, magnitude, and systemic velocity, de Vaucouleurs (1959) assigned it to the nearby Sculptor group, but as one of the faintest members it has largely escaped attention. The only previous kinematic study has been made by Rogstadt, Rougoor, and Whiteoak (1967) using a single spacing of the Owens Valley interferometer.

The present paper reports the results of observations of NGC 45 at 21 cm wavelength using the 210 ft radio telescope at Parkes. This is the smallest galaxy so far studied with the Parkes telescope at this wavelength; its optical dimensions of $7'{\cdot}4\times5'{\cdot}1$ are small compared with the 3 dB beamwidth of $14'{\cdot}5$. Spectra are presented here for a grid of 44 points spaced at 6′ intervals across the galaxy. Sections III and IV contain the details of the HI mass, its distribution, and the observed velocity field, while Sections V and VI give details of the model simulation and the corrected rotation curve.

## II. Observing Equipment and Procedure

A quasi-degenerate parametric amplifier, designed and built by M. W. Sinclair, was used as the first stage. It was coupled to a crystal mixer and thence to a conventional 48-channel 21 cm switched-frequency line receiver. The amplifier had 40 dB of isolation from all the following stages and used a 2851 MHz klystron pump, which was phase-locked to a quartz-crystal oscillator. McGee and Murray (1963) have described the rest of the receiver, while Hindman *et al.* (1963) have given the details of the digital recording and data handling. Each of the double tuned *LC*

* Mount Stromlo and Siding Spring Observatories, Research School of Physical Sciences, Australian National University; present address: Nuffield Radio Astronomy Laboratories, Jodrell Bank, England.

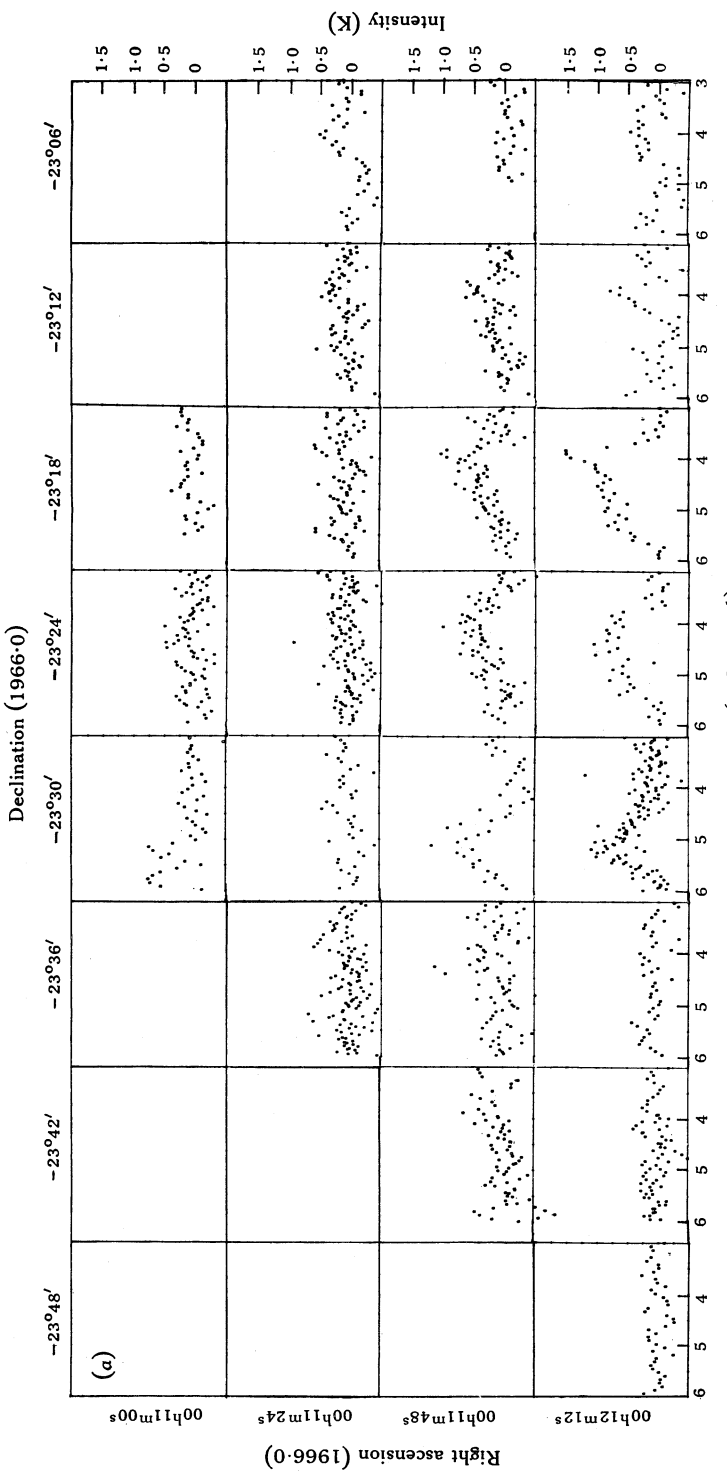
(a)
Declination (1966·0)
−23°48′
−23°42′
−23°36′
−23°30′
−23°24′
−23°18′
−23°12′
−23°06′
Right ascension (1966·0)
00h11m00s
00h11m24s
00h11m48s
00h12m12s
Intensity (K)
1·5
1·0
0·5
0
Radial velocity (10² km s⁻¹)
3
4
5
6

Fig. 1(*a*)

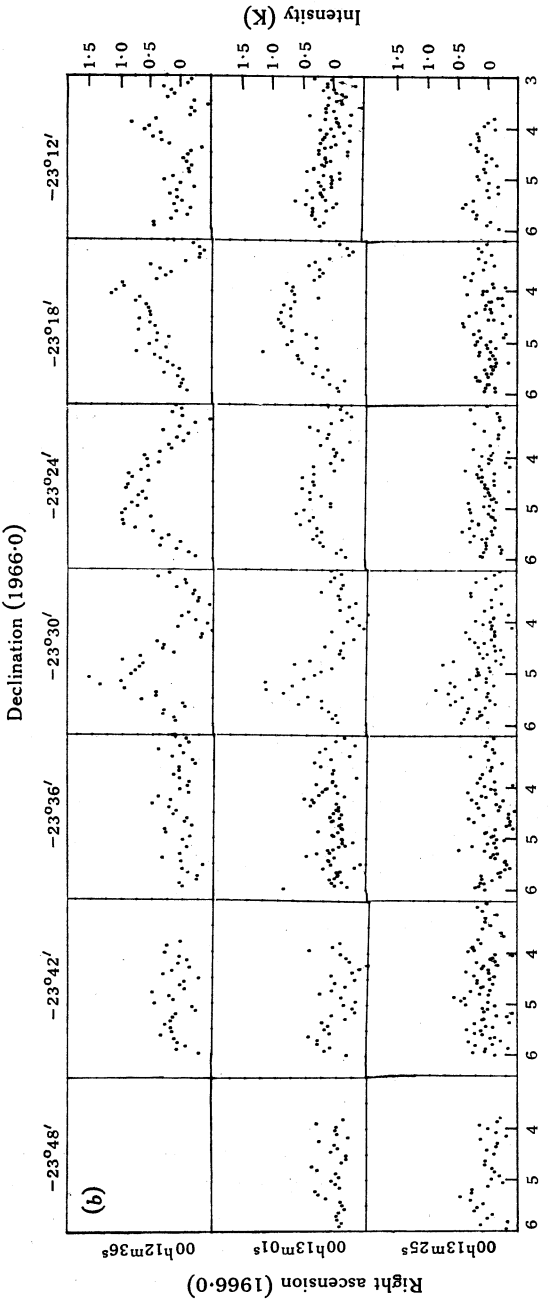


Fig. 1.—Grid of 44 selected profiles across NGC 45. The velocities are with respect to the local standard of rest.

filters has a 3 dB bandwidth of 37 kHz and an output to a two-stage $RC$ integrator with a 2 min time constant.

Generally observations were made using a 2·5 MHz difference between the signal and reference frequencies. While this caused a 440 km s$^{-1}$ separation between the centres of each of the observed bands, their closest channels were still separated by 100 km s$^{-1}$. Since the typical signal was $\sim 0{\cdot}5$ K, the observations were made by integrating for eight minutes at a time on each position. Four minutes were allowed to elapse unrecorded after every change of telescope position, thus ensuring that the output time constants were not affected by the previous signal. Most of the spectra used here were recorded in September 1967, when the system noise temperature was 350 K and the r.m.s. noise fluctuation was 0·26 K. Spectra were generated from the source profiles by subtracting the profiles of reference regions which had been recorded immediately before or after in time at positions taken 12 min of time east or west of the last observed source position. The individual channel gains were regularly measured with a noise lamp.

Following Robinson and van Damme (1966), the sensitivity of the antenna–receiver system was measured using 3C 353. It was found that the aerial response with a scalar feed could be represented with good accuracy by a circularly symmetric Gaussian of width $\sigma_{\text{beam}} = 6'{\cdot}17$ and that the pointing errors were within $\pm 1'$ arc. The effective solid angle of the beam $\Omega_{\text{b}}$ (Seeger, Westerhout, and van de Hulst 1956) was 238 sq min and the beam efficiency $(1-\chi)$ was 0·80.

## III. HI Distribution

The data tapes were reduced off line using standard CSIRO programs. After correlating with the position tape and applying the channel gain calibration, the spectra were plotted on a velocity scale corrected to the local standard of rest. Figures 1($a$) and 1($b$) show the grid of 44 selected spectra in this form. Neutral hydrogen was detected over the velocity range 350–550 km s$^{-1}$, with a peak intensity of 1·5 K at the position $00^{\text{h}}12^{\text{m}}12^{\text{s}}$, $-23°18'$. Preliminary observations of NGC 45 were made over most of the central regions using the single-channel receiver described by Robinson and van Damme (1966).†

The simplest way of describing the HI distribution is to isolate it from the velocity field by measuring the area under every spectrum. This defines the integrated antenna temperature

$$T_{\text{A}}(\theta,\phi) = \int_{\nu} T_{\text{a}}(\theta,\phi,\nu)\,\mathrm{d}\nu\,.$$

Any value of $T_{\text{A}}$ measured at a position $(\theta,\phi)$ is sensitive to both noise and baseline instabilities as well as to errors in drawing the baseline. An estimated standard error of 20% was assumed in drawing the contour diagram in Figure 2. It can be seen that the HI centroid is displaced by $\sim 2'$ to the south-west along the minor axis. By defining an effective radius $r^*$ of a contour $T_{\text{A}}$ from the area $A(T_{\text{A}})$ within

† A tabulation of the peak velocities of all spectra together with the positions and quality weightings may be obtained on application to the Editor-in-Chief, Editorial and Publications Section, CSIRO, 372 Albert Street, East Melbourne, Vic. 3002.

it through the relation

$$r^* = \{\pi^{-1} A(T_A)\}^{\frac{1}{2}}, \tag{1}$$

the effective variation of $T_A$ with radius can be measured. In Figure 3 the data are plotted with the best-fitting Gaussian of half-width $\sigma^*$. An approximate correction was made to $\sigma^*$ to remove the effects of beam smoothing and foreshortening using the formula

$$\sigma_r = \{(\sigma^{*2} - \sigma^2_{\text{beam}})/\cos i\}^{\frac{1}{2}}, \tag{2}$$

where $\sigma_r$ is a convenient measure of the size of the intrinsic HI distribution and

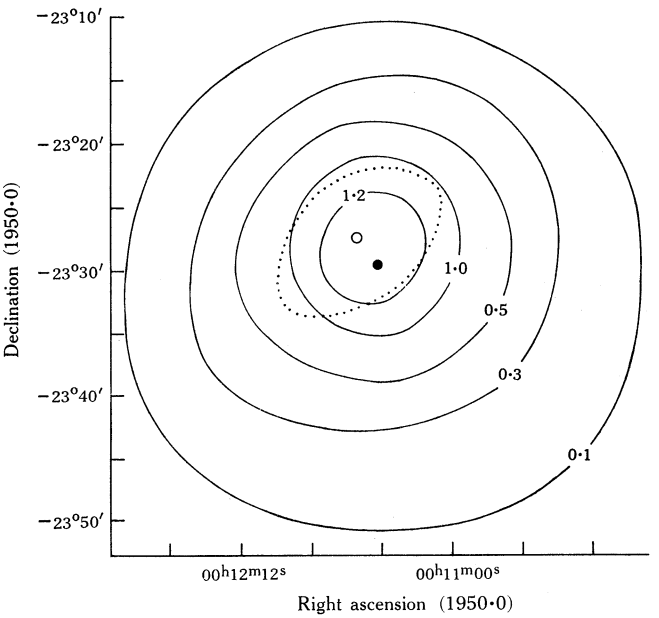


Fig. 2.—Contours of integrated antenna temperature $T_A$ over NGC 45. The contours are equivalent to brightness temperatures in units of $10^3$ K.km s$^{-1}$. The dotted curve shows the limits of the brighter optical regions, the optical centre (O) being displaced by 2′·0 from the HI centroid (●).

$i$ is the angle between the plane of the galaxy and the plane of the sky. This 21 cm size is compared with the optical size $D(O)$ given by de Vaucouleurs and de Vaucouleurs (1964) through the ratio $2\sigma_r/D(O) = 2 \times 6' \cdot 9/7' \cdot 4 = 1 \cdot 86$, which is close to the average found for most late type galaxies (Lewis and Robinson 1972).

Provided the optical depth $\tau$ is small, the HI mass can be evaluated from the well-known equation (Robinson and van Damme 1966)

$$M_H/M_\odot = 3 \cdot 1 D^2 (1-\chi)^{-1} \iiint_c T_a(\theta, \phi, \nu)\, d\theta\, d\phi\, d\nu, \tag{3}$$

in which $D$ is expressed in kiloparsecs and $\nu$ in hertz and the integration is performed

over the whole region of the convolution of the galaxy with the aerial response $A(\xi, \eta)$. Planimetry of Figure 2 gives an HI mass of $7{\cdot}6 \times 10^8 M_\odot$. When the Gaussian fitted to the mean radial distribution of $T_A$ is extrapolated from the last observed contour to $r = \infty$, the HI mass is increased by 8% to $8{\cdot}2 \times 10^8 M_\odot$.

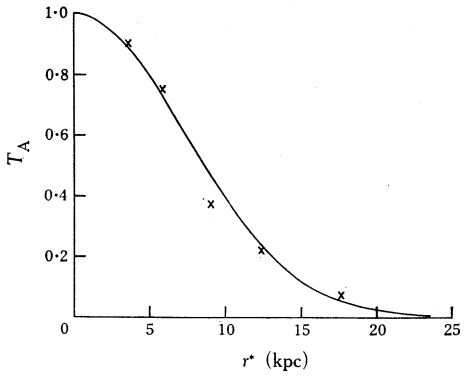


Fig. 3.—Comparison of the best-fitting Gaussian, of half-width $\sigma^* = 8'{\cdot}1$ ($\equiv 7{\cdot}0$ kpc), with the integrated antenna temperature $T_A$. (To express $T_A$ in units of $10^3$ K km s$^{-1}$ multiply by 13·8.)

## IV. Observed Velocity Field

Provided the HI is confined to a thin disk in the plane of the galaxy and the velocity field is circularly symmetric about the rotation centre, the observed distribution of peak velocities can be described by a rotation curve $\Phi(r)$. The transformation from the observed velocity at $(\rho, \phi)$ in the plane of the sky to $(r, \psi = 0 \text{ or } \pi)$ in the plane of the galaxy is then through the equations

$$V_{\text{obs}} = V_0 + \Phi(r) \cos\psi \sin i\,, \tag{4}$$

$$r = \rho(1 + \sin^2\phi \tan^2 i)^{\frac{1}{2}}\,, \tag{5}$$

$$\psi = \arctan(\tan\phi \sec i)\,, \tag{6}$$

in which the azimuthal angles are measured with respect to the major axis position angle $\phi_0$ and $V_0$ is the systemic velocity. Figure 4 shows the resulting rotation curve. All observations within $\Delta\psi = \pm 80°$ of the major axis are plotted. To distinguish those observations in Figure 4 for which the projection factors are small, the quality weighting is multiplied by $\cos^2\psi/(1 + \sin^2\phi \tan^2 i)^{\frac{1}{2}}$ and the observations with a weight $w$ in excess of 0·6 are then shown as solid circles. The crosses indicate the interferometer observations of Rogstadt, Rougoor, and Whiteoak (1967). They agree in form with the mean curve defined by the present data.

When a five point running mean is made of the data plotted in Figure 4 after the points are ordered monotonically by their radii, the low weight data between $r = 15'$ and $20'$ on the south-east branch show a local minimum. An asymmetry of this form was also found in NGC 4027 (de Vaucouleurs, de Vaucouleurs, and Freeman 1968). Despite this apparent asymmetry, when a Brandt (1960) function is fitted separately to the data from each side of the minor axis, the resulting curves are symmetrical within the standard errors of the fit.

Since the number of the independent observations along the major axis was small, a Brandt function $\Phi(r)$ of predetermined index $n$ was fitted to the observed

velocity field by the method of least squares (Deming 1943) using (4) as the normal equation. The Brandt function has the form

$$\Phi(r) = V_M 3^{3/2n}(r/R_M)/\{1+2(r/R_M)^n\}^{3/2n}, \quad (7)$$

where $(R_M, V_M)$ are the coordinates of the turnover point. In fitting the observed velocity field, there are errors in the estimation of the position $(\rho, \phi)$ as well as in the peak velocity, due to the intrinsic clumpiness of the HI distribution, the effects

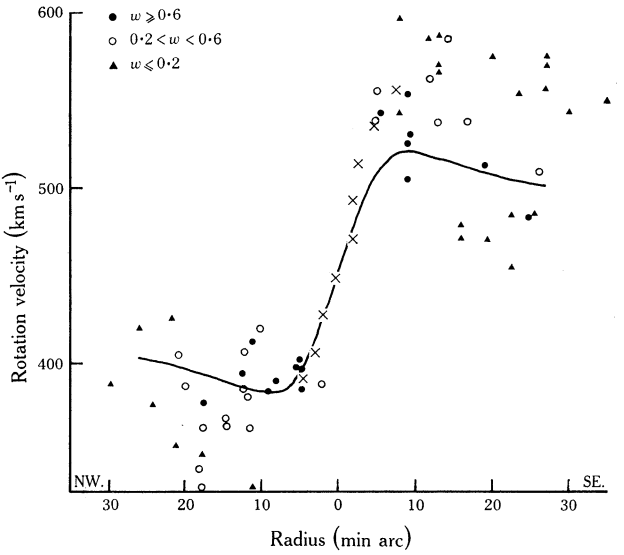


Fig. 4.—Rotation curve of NGC 45 obtained from the uncorrected data after projection onto the major axis ($\phi_0 = 145°$, $i = 55°$). The weight $w$ of the observations is indicated. The crosses show the interferometer data of Rogstadt, Rougoor, and Whiteoak (1967).

TABLE 1

LEAST SQUARES FIT OF BRANDT FUNCTION TO OBSERVED DATA

Parameter values: $\sigma_\rho = 2'$; $\sigma_{vel} = 15$ km s$^{-1}$; $i = 55°$; $V_0$ (w.r.t. Sun) = 459 km s$^{-1}$; position of centre (1950·0) = $00^h\,11^m\,31^s$, $-23°\,27'{\cdot}4$; $\phi_0 = 145°$; $\Delta\psi = \pm 30°$

| Field | No. of Obs. | $n$ | $V_M$ (km s$^{-1}$) | $R_M$ (min arc) | $\sigma_r^2$ |
|---|---|---|---|---|---|
| Following | 11 | 3 | 83±121 | 9·2±6·5 | 0·78 |
| Preceding | 8 | 3 | 87±32 | 9·0±1·7 | 0·29 |
| Total | 19 | 3 | 85±38 | 8·9±1·7 | 0·52 |

of beam smoothing, and the assumption of definite values for $V_0$, $i$, $\phi_0$, $n$, and the position of the rotation centre. The fit was therefore made with allowance for errors in $V_{obs}$, $\rho$, and $\phi$ by defining standard errors for these parameters as $\sigma_{vel} = 15$ km s$^{-1}$, $\sigma_\rho = 2'$, and $\sigma_\phi = 2/\rho$. Using equations (5) and (6), the standard errors in $r$ and $\psi$ are then

$$\sigma_r^2 = \{(1+\sin^2\phi\tan^2 i)^2+\sin^2\phi\tan^4 i\}\sigma_\rho^2/(1+\sin^2\phi\tan^2 i) \quad (8)$$

and

$$\sigma_\psi = \cos^2\psi\sec^2\phi\sec i\,\sigma_\phi\,. \quad (9)$$

Table 1 shows the results of fitting a Brandt function directly to the observed velocity field. Trial solutions were made with many different sets of adopted constants to ensure that a genuine minimum had been found in the sum of the squares of the

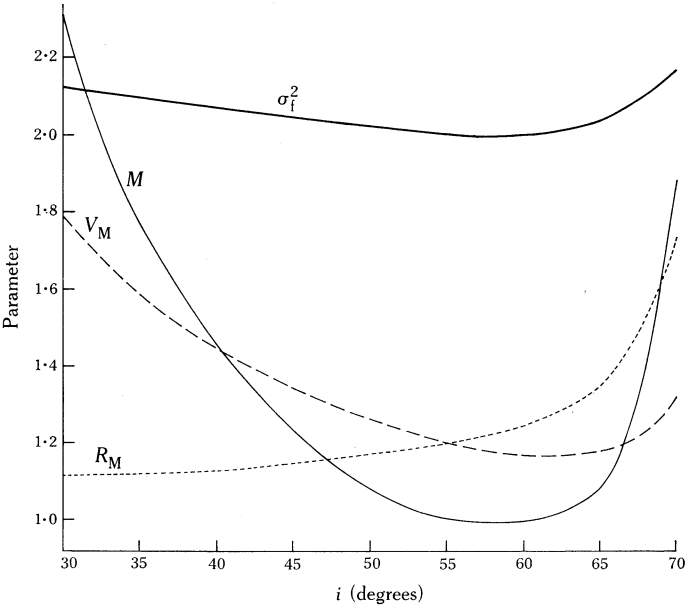


Fig. 5.—Variation of $\sigma_f^2$ and the fitted parameters $R_M$, $V_M$, and the total mass $M$ with the inclination $i$, the most difficult parameter to determine accurately. All curves are normalized to 1·00 at $i = 55°$ but are plotted with arbitrary offsets on the ordinate scale for clarity.

TABLE 2

COMPARISON OF VALUES OF $V_0$, $i$, AND $\phi_0$ FROM DIFFERENT METHODS

| Systemic velocity $V_0$ (w.r.t. Sun) (km s$^{-1}$) | Major axis P.A. $\phi_0$ (deg) | Inclination $i$ (deg) | Method |
|---|---|---|---|
| 450±50 | — | 47 | Optical* |
| 459±5 | 145±5 | 55±5 | 21 cm, kinematic |
| 470† | 125±15 | — | 21 cm, integrated $T_a$ contours |
| — | 145±15 | 54 | Mean optical isophotes |
| — | 145 | 58 | Limiting isophote |
| 459±5 | 145±5 | 55±3 | Adopted values |

* de Vaucouleurs and de Vaucouleurs (1964).
† Rogstadt, Rougoor, and Whiteoak (1967).

weighted residuals. Figure 5 shows the smooth variation of $\sigma_f^2$, the square of the standard error of the fit, as a function of the inclination $i$ together with the variation of $V_M$, $R_M$, and $M = V_M^2 R_M$. Kinematic estimates of $\phi_0$, $i$, and $V_0$ can be derived by separately varying each, and these values are in excellent agreement with the results from other methods as indicated in Table 2.

The optical estimates of $\phi_0$ and $i$ were made from measurements of a 103a–O plate of NGC 45 taken with the Mount Stromlo 74 in. telescope. Contours of equal density increments above the plate background were constructed from microphotometer tracings and the value of $\phi_0$ was then found from a plot of the diameter as a function of $\phi$. The inclination was estimated from the ratio of the axes $b/a$ using the relation

$$\cos i = 1{\cdot}02\{(b/a)^2 - 0{\cdot}04\}.$$

Though tests were also made with a number of alternative rotation centres, none gave a better fit than the Glanfield and Cameron (1967) position.

## V. Model Simulation

If the mean velocity of the HI in any small region of a galaxy is taken to be the characteristic velocity of that position, then large errors are incurred in accepting the peak velocity of a profile as the characteristic velocity of the position in the galaxy which lies on the principal axis of the beam, whenever the source is comparable in size with the beam. These errors can be most reasonably evaluated by constructing model galaxy profiles to compare directly with the observations. The results of such a procedure are not unique and are strongly conditioned by the model used.

Model galaxies have previously been constructed by Burke, Turner, and Tuve (1964), Epstein (1964), and Roberts (1968). For simplicity the velocity field is usually assumed to follow a circularly symmetric Brandt function, while the HI is confined to the plane of the galaxy, is smoothly distributed, and has a spin temperature $T_s = 120\,\mathrm{K}$. It was seen in Section III that a Gaussian distribution adequately represents the radial distribution of HI, and so the number density at a radius $r$ in the plane of the galaxy is given by

$$N_{\mathrm{H}}(r) = N_0 \exp(-r^2/2\sigma_r^2) \sec i = \int_{-\infty}^{\infty} n_{\mathrm{H}}\, \mathrm{d}s, \tag{10}$$

where $n_{\mathrm{H}}$ is the space density of the hydrogen and $s$ is the distance along the line of sight. When the total HI mass $M_{\mathrm{H}}$ is expressed in solar masses, $\sigma_r$ in minutes of arc, and the distance $D$ in megaparsecs,

$$N_0 = (M_{\mathrm{H}}/\sigma_r^2 D^2) \times 2{\cdot}502 \times 10^{14} \quad \text{atoms cm}^{-2}.$$

If the random HI velocities in a galaxy are assumed to be isotropic and Gaussian with a velocity dispersion $\sigma_{\mathrm{v}}$, after convolution with the $i$th filter of width $\sigma_{\mathrm{b}}$ centred on $V_i$, the mean opacity $\bar{\tau}$ is related to the number density by

$$\bar{\tau}(\theta, \phi, V_i) = \frac{5{\cdot}45 \times 10^{-19} N_{\mathrm{H}}(r)}{T_s\, \sigma_{\mathrm{c}} (2\pi)^{\frac{1}{2}}} \exp\left(-\frac{(V_i - V)^2}{2\sigma_{\mathrm{c}}^2}\right), \tag{11}$$

in which $\sigma_{\mathrm{c}}^2 = \sigma_{\mathrm{v}}^2 + \sigma_{\mathrm{b}}^2$ and $V$ is the characteristic velocity at $(\theta, \phi)$. The antenna temperature $T_{\mathrm{a}}$ is numerically evaluated from the relation (Baars, Mezger, and Wendker 1965)

$$T_{\mathrm{a}}(\theta, \phi, V_i) = (1 - \chi) T_s\, \Omega_s(\theta, \phi, V_i)/\Omega_{\mathrm{b}}, \tag{12}$$

where

$$\Omega_s(\theta, \phi, V_i) = A_0^{-1} \iint [1 - \exp\{-\bar{\tau}(\xi - \theta, \eta - \phi, V_i)\}] A(\xi, \eta)\, d\xi\, d\eta \qquad (13)$$

with

$$A_0 = \lambda^2(1-\chi)/\Omega_b .$$

Once the orientation of the model and the parameters $\Omega_b$, $(1-\chi)$, and $\sigma_b$ of the observing system are specified, model profiles can be constructed for any given rotation curve after adopting some value for $\sigma_v$, $\sigma_r$, and $N_0$. A comparison is made in Figure 6

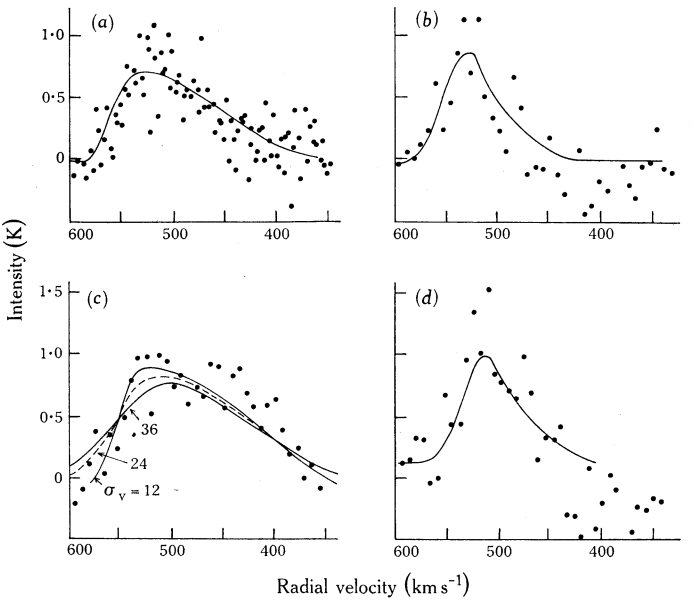


Fig. 6.—Comparison between the model profiles and the data for four of the spectra in Figure 1: (*a*) $X = 5'{\cdot}4$, $Y = 6'{\cdot}0$; (*b*) $11'{\cdot}8$, $-3'{\cdot}0$; (*c*) $3'{\cdot}7$, $-1'{\cdot}5$; (*d*) $8'{\cdot}6$, $1'{\cdot}5$. The velocities are relative to the local standard of rest. In the most central profile (*c*) alternative fits are shown for velocity dispersions $\sigma_v$ of 12, 24, and 36 km s$^{-1}$.

between four computed and observed spectra. No separate scaling is applied to the model profiles, except that which occurs in the course of determining the best self-consistent values for $\sigma_v$ and the rotation curve. It can be seen that the model spectra agree best with the observations taken at a little distance from the nucleus. This is due to the adoption of a constant value of $\sigma_v$ over the whole galaxy. Alternative fits with $\sigma_v = 24$ and 36 km s$^{-1}$ are shown for the most central profile (Fig. 6(*c*)); the intense channels and the sharp rise at a velocity of $\sim 540$ km s$^{-1}$ are best described by $\sigma_v = 12$ km s$^{-1}$, while the broader low intensity wings are fitted better with $\sigma_v \sim 30$ km s$^{-1}$.

Care was taken to evaluate equation (13) on a sufficiently fine grid of positions. Usually a grid of $25 \times 25$ points with a spacing of $2'$ along the major axis was sufficient

to generate smooth profiles, and when four times as many points were evaluated with their spacing halved there was in general no sensible modification of the form of the model profiles. However, the rather small scale of NGC 45 with the rotation curve peaking at a radius of only 7′ necessitated the central profiles ($r < 8'$) being calculated on the finer grid.

The distortions of the velocity field by beam smoothing are shown by Figure 7, in which peak velocities of model profiles on the major axis are compared with the adopted rotation curve. Beam smoothing reduces the size of $V_M$ while increasing $R_M$ and reducing the velocity gradient for $r > R_M$. Thus, after correcting the velocity data of NGC 45, these trends result in a Brandt function of $n = 10$ giving a better

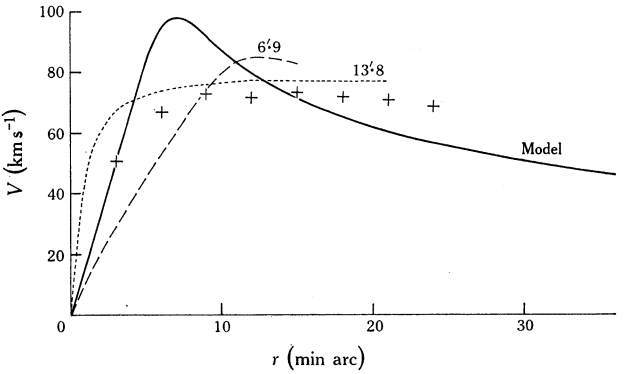


Fig. 7.—Distortions introduced by beam smoothing are shown by the divergence of the peak velocities of model profiles on the major axis (plotted as crosses) from the adopted rotation curve; with perfect resolution the peak velocities lie on the model curve. Also shown for comparison are similar rotation curves obtained from models in which the HI distribution is constant over disks of radii 6′·9 and 13′·8 but is zero elsewhere.

fit than the $n = 3$ curve fitted to the uncorrected data. It is therefore necessary to apply a substantial correction to the observed velocity field to achieve realistic rotation curves. The pattern of these corrections for the high velocity end of NGC 45 is shown in Table 3. Each correction has been determined from the difference between the peak velocity of a model profile calculated with the set of parameters listed in Table 4, and the velocity predicted by the adopted rotation curve at the same position. For example, entering Table 3 at $X = 9'$, $Y = 0'$ gives a correction of $+21$ km s$^{-1}$ to the peak velocity of 73 km s$^{-1}$ at this position, thus adjusting the peak velocity to the 94 km s$^{-1}$ predicted by the adopted rotation curve. The effect of these corrections on the major axis $X$ can be seen in Figure 7 to translate the simulated observational curve shown by the sequence of crosses into the model curve. The velocity corrections required at the actual observed positions have been obtained by interpolation from Table 3; the sign of the correction changes for the low velocity end of NGC 45.

It is worth noting that the size of the corrections in Table 3 is at most 40% of the peak velocity, and characteristically of the order of 25–30% over most of the

plane. The magnitude of the corrections would be increased in a smaller object of larger inclination, but the relative size is held in check here by the change in sign when moving out along both the major and minor axes, and by the small gradients in HI density and velocity beyond $r = 7'$. Since the pattern of these corrections is

TABLE 3

VELOCITY CORRECTIONS FOR BEAM SMOOTHING

$X$ = major axis, $Y$ = minor axis

| | Velocity correction (km s$^{-1}$) | | | | | | | | |
|---|---|---|---|---|---|---|---|---|---|
| $Y$ | $X = 0'$ | $3'$ | $6'$ | $9'$ | $12'$ | $15'$ | $18'$ | $21'$ | $24'$ |
| $0'$ | 0 | 0 | 29 | 21 | 10 | 0 | −5 | −9 | −12 |
| $3'$ | 0 | 2 | 8 | 3 | 0 | −7 | −8 | −11 | −13 |
| $6'$ | 0 | −5 | −28 | −24 | −17 | −16 | −16 | −17 | −17 |
| $9'$ | 0 | −6 | −39 | −32 | −30 | −27 | −25 | −23 | −22 |
| $12'$ | 0 | −7 | −19 | −29 | −31 | −30 | −27 | −25 | −23 |
| $15'$ | 0 | −8 | −17 | −23 | −26 | −26 | −27 | −26 | −25 |

distinctive and symmetrical about the major and minor axes, the kinematic fit to the uncorrected observations is minimized best by choosing the true major axis. The accuracy of this technique is thus often due to the relatively large size of the beam-smoothing corrections.

TABLE 4

PARAMETERS OF NGC 45

| Parameter | Value | Parameter | Value |
|---|---|---|---|
| R.A. (1950·0)* | $00^h\,11^m\,31^s$ | $V_M$ | 121 km s$^{-1}$ |
| Dec. (1950·0)* | $-23°\,27'·4$ | $R_M$ | $6'·9$ |
| Type† | SA(s) dm | Total mass $M$ | $2·5\times10^{10}\,M_\odot$ |
| Distance‡ | 3 Mpc | Apparent magnitude | $10·6^m$ |
| Systemic velocity $V_0$ (w.r.t. Sun) | 459 km s$^{-1}$ | Absorption-free luminosity $L$ | $1·6\times10^9\,L_\odot$ |
| Major axis position angle $\phi_0$ | 145° E. of N. | $M/L$ | 15·6 |
| Inclination $i$§ | 55° | $m_H/M$ | 0·033 |
| Velocity dispersion $\sigma_V$ | $12\pm6$ km s$^{-1}$ | $m_H/L$ | 0·513 |
| Gaussian HI dispersion $\sigma_r$ | $6'·9$ | Solid angle of beam ($\Omega_b$) | 238 sq min |
| Spin temperature $T_s$ | 120 K | Beam efficiency ($1-\chi$) | 0·80 |
| Hydrogen mass $m_H$ | $8·2\times10^8\,M_\odot$ | Observing bandwidth ($\sigma_b$) | 15·7 kHz |
| Brandt index $n$ | 10 | Beam half-width | $14'·5$ |

* Glanfield and Cameron (1967). † de Vaucouleurs (1959).
‡ Lewis and Robinson (1972). § $i = 90°$ is edge on.

Self-consistent model galaxies were reached by updating the initial rotation curve fitted to the uncorrected data. This generated a set of corrections similar to those in Table 3 which, when applied to the observations, allowed a more accurate rotation curve to be fitted. Usually one repetition of this process was sufficient to

generate a self-consistent model. The form of Table 3 was found to be rather insensitive to small changes in $\sigma_r$ or in the position of the HI centroid. All models were therefore constructed assuming a Gaussian HI distribution with $\sigma_r = 6'{\cdot}9$. It is possible to estimate the acceptable range of $\sigma_V$ by constructing a sequence of models and judging the suitability from the size of the standard error of the fitted rotation curve. Thus $\sigma_V = 18$ km s$^{-1}$ gives a 15% worse fit than $\sigma_V = 12$ km s$^{-1}$.

TABLE 5

LEAST SQUARES FIT OF BRANDT FUNCTIONS TO CORRECTED DATA

Parameter values as for Table 1

| $n$ | $V_M$ (km s$^{-1}$) | $R_M$ (min arc) | Total mass ($10^{10} M_\odot$) | $\sigma_f^2$ |
|---|---|---|---|---|
| 3 | 109±27 | 6·23±0·53 | 2·40±1·37 | 0·363 |
| 5 | 113±28 | 6·71±0·46 | 2·38±1·32 | 0·331 |
| 10 | 121±30 | 6·92±0·35 | 2·49±1·37 | 0·311 |
| 20 | 131±31 | 7·03±0·21 | 2·79±1·40 | 0·303 |

## VI. MASS OF NGC 45

After applying the corrections listed in Table 3, the observations within $\Delta\psi = \pm 30°$ of the major axis were fitted to a Brandt function of index $n$. Table 5 shows the resulting parameters together with their standard errors for a number of different values of $n$. All points at $r > 25'$ are excluded since the predicted peak temperatures are then comparable with the departures from linearity in the baselines. Figure 8 shows some of the fitted curves together with the corrected data after projection onto the major axis.

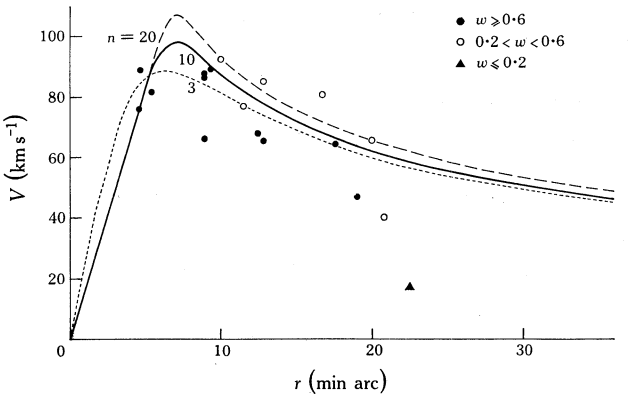


Fig. 8.—Comparison of the corrected observations within 30° of the major axis after projection onto this axis with the fitted rotation curves for three values of the Brandt function index $n$. The weight $w$ of the observations is indicated.

It is interesting to compare the present results with the more approximate values obtained by Rogstadt, Rougoor, and Whiteoak (1967) using only a single spacing of the Owens Valley interferometer. From their models with a different rotation centre and assuming $n = 3$, they estimated $V_M(i = 50°) = 110$ km s$^{-1}$ and $R_M \simeq 6'{\cdot}5$, values which are very close to those listed in Table 5 for $n = 3$, and not dissimilar to the $n = 10$ results of $V_M(i = 55°) = 121$ km s$^{-1}$ and $R_M = 6'{\cdot}92$. This is important confirmation of the accuracy of the procedures used here in adjusting

the data for the effects of beam smoothing and shows that meaningful results can be obtained for galaxies with 21 cm dimensions comparable with the beam.

Total masses estimated to an infinite radius and adjusted upwards by 10% to allow for the finite thickness of the disk were calculated from the relation due to Roberts (1968)

$$M/M_{\odot} = 72 \cdot 6(3/2)^{3/n} V_{\mathrm{M}}^2 R_{\mathrm{M}} D,$$

where $V_{\mathrm{M}}$ is in km s$^{-1}$, $R_{\mathrm{M}}$ in minutes of arc, and $D$ in kiloparsecs. For $n = 10$, the resulting total mass is

$$M = (2 \cdot 49 \pm 1 \cdot 37) \times 10^{10} M_{\odot}.$$

The sensitivity of this result to the form of the rotation curve used can be seen in Table 5, which shows a small increase in the estimated mass as $n$ increases in value. Improvements in resolution may show a more rapid decrease of rotation velocity with radius and a slight increase in the total mass. If the mass is estimated from the fitted rotation curve out as far as the last well-observed data at $r = 18'$, the mass is $M(r < 18') = 2 \cdot 12 \times 10^{10} M_{\odot}$. This agrees closely with the Keplerian mass estimated from the same position ($r = 18'$, $V(r) = 59 \operatorname{cosec} 55°$) of $2 \cdot 09 \times 10^{10} M_{\odot}$. Thus 85% of all the mass lies within this radius.

## VII. Acknowledgments

I wish to thank Dr. B. J. Robinson for the many interesting discussions about the problems encountered in bringing this work to a conclusion, and for his unstinted encouragement. I am also much obliged to Mr. J. G. Bolton for permission to use the Parkes 210 ft telescope and to the staff of the Division of Radiophysics, CSIRO, for their help with the observing. Most of this work was done with the support of an A.N.U. Postgraduate Scholarship. The manuscript has been prepared during the tenure of a Research Fellowship at Jodrell Bank.

## VIII. References

Baars, J. W. M., Mezger, P. G., and Wendker, H. (1965).—*Astrophys. J.* **142**, 122.
Brandt, J. C. (1960).—*Astrophys. J.* **131**, 293.
Burke, B. F., Turner, K. C., and Tuve, M. A. (1964).—*Yb. Carnegie Instn Wash.* **63**, 341.
Deming, W. E. (1943).—"Statistical Adjustment of Data." (Wiley: New York.)
Epstein, E. E. (1964).—*Astr. J.* **69**, 521.
Glanfield, J. R., and Cameron, M. J. (1967).—*Aust. J. Phys.* **20**, 613.
Hindman, J. V., McGee, R. X., Carter, A. W. L., Holmes, E. C. J., and Beard, M. (1963).—*Aust. J. Phys.* **16**, 552.
Lewis, B. M., and Robinson, B. J. (1972).—The Sculptor group. *Astr. Astrophys.* (in press).
McGee, R. X., and Murray, J. D. (1963).—*Proc. Inst. Radio Engrs Aust.* **24**, 191.
Roberts, M. S. (1968).—*Astrophys. J.* **151**, 117.
Robinson, B. J., and van Damme, K. J. (1966).—*Aust. J. Phys.* **19**, 111.
Rogstadt, D. H., Rougoor, G. W., and Whiteoak, J. B. (1967).—*Astrophys. J.* **150**, 9.
Sandage, A. (1961).—"The Hubble Atlas of Galaxies." (Carnegie Instn: Washington.)
Seeger, C. L., Westerhout, G., and van de Hulst, H. C. (1956).—*Bull. astr. Insts Neth.* **13**, 89.
de Vaucouleurs, G. (1959).—*Astrophys. J.* **130**, 718.
de Vaucouleurs, G., and de Vaucouleurs, A. (1964).—"Reference Catalogue of Bright Galaxies." 1st Ed. (Texas Univ. Press.)
de Vaucouleurs, G., de Vaucouleurs, A., and Freeman, K. C. (1968).—*Mon. Not. R. astr. Soc.* **139**, 425.